PHYSICAL REVIEW B **79**, 024432 (2009)

Nonlinear magnetoelastic coupling of epitaxial layers of Fe, Co, and Ni on Ir(100)

Zhen Tian, Dirk Sander, and Jürgen Kirschner
Max-Planck-Institut für Mikrostrukturphysik, Weinberg 2, D-06120 Halle/Saale, Germany
(Received 4 November 2008; published 30 January 2009)

The effective magnetoelastic coefficients B_i^{eff} are measured for epitaxial layers of Fe, Co, and Ni on Ir(100). Mechanical stress during film growth and stress during magnetization processes are measured directly by the optical cantilever curvature technique. Our results indicate that the effective magnetoelastic coupling coefficients B_1^{eff} and B_2^{eff} of Fe, Ni, and Co deviate from the respective bulk values, and we propose that strain may play an important role for this nonbulklike magnetoelastic behavior. The impact of the magnetoelastic coupling on the magnetic anisotropy is explored by magneto-optic Kerr effect measurements. The measurements reveal that the easy magnetization axis is in plane for Fe and Co layers on Ir(100). It changes from out of plane to in plane for Ni at about 15 monolayer with increasing film thickness. This spin reorientation transition can be well described by the measured magnetoelastic coupling coefficients. The result of nonbulklike magnetoelastic coupling is discussed in view of recent theoretical work on the calculation of magnetoelastic coupling in strained systems.

DOI: 10.1103/PhysRevB.79.024432 PACS number(s): 75.80.+q, 75.70.Ak, 75.30.Gw, 68.60.Bs

I. INTRODUCTION

The magnetic properties of ferromagnetic epitaxial layers and nanostructures often deviate from that of their bulk counter parts.[1,2,4–9] A most intriguing aspect is the change in the easy magnetization direction away from that of the respective bulk sample.[10–15] One important issue in understanding the physical principle behind this change in magnetic anisotropy on the nanoscale is how the almost inevitable lattice strain of the nanostructure or ferromagnetic film couples to the magnetic anisotropy.[12,16–20] This link between lattice strain and magnetic anisotropy is given by the magnetoelastic (ME) coupling, which is defined as the strain derivative of the magnetic anisotropy energy.[21]

An intriguing result of recent experimental and theoretical works is that lattice strain changes the magnetoelastic coupling. For Fe monolayers on W(100) even a change in sign of the magnetoelastic coupling coefficients as compared to bulk Fe has been found.[12] Theory predicts a nontrivial impact of lattice strain on the magnetic anisotropy.[22] Whereas magnetoelastic bulk behavior should induce a linear relation between magnetic anisotropy energy and lattice strain, calculations identify the importance of higher-order strain contributions.[23] Theory indicates that the magnetic anisotropy changes with lattice strain in a nonmonotonic manner.[22] Thus, both experiment and theory indicate that the application of bulk magnetoelastic coupling coefficients may not be appropriate to predict the magnetic anisotropy of strained films.[12]

Qualitatively, the electronic origin of the magnetic anisotropy is based on the coupling of the electron-spin magnetic moment to the crystal lattice as expressed by the relativistic spin-orbit coupling (SOC).[3,4] The intrinsic complexity of magnetic anisotropy and its small energy scale of order of 1 μeV per atom in cubic transition-metal atoms render very demanding calculations of magnetoelastic effects due to the required high numerical accuracy.[4]

Highly accurate calculations of the spin-resolved electronic structure and its dependence on strain are required to treat magnetoelastic effects, and they have been performed for selected examples.[22–27] These theoretical works and experiments[28] have clearly shown that the loss of cubic symmetry of an epitaxially strained system is correlated with a change in the magnetic anisotropy energy by orders of magnitude.

Relativistic electronic structure calculations have revealed that strain-induced topological changes in the Fermi surface are decisive for the understanding of magnetoelastic coupling in strained systems.[22,26,27] However, a clear understanding has not emerged yet which allows a prediction on the effective magnetoelastic coupling in ultrathin films and nanostructures in general. This shortcoming is also due to the very limited experimental database which serves as a comparison for calculations. In cases where both experimental and theoretical data are available the agreement between experiment and theory is often qualitative at best. Theory and experiment are also found to disagree in other cases.[27]

In order to contribute to a better understanding of magnetoelastic effects, we present here experimental data on the magnetoelastic coupling in strained epitaxial layers of Fe, Co, and Ni on Ir(100). We discuss the results in view of *in situ* stress measurements and structural investigations. We find in all cases that the magnetoelastic coupling of the layers deviates from the respective bulk value. Our combined stress and structural investigations identify lattice strain as an important factor for the modified magnetoelastic coupling in epitaxially strained layers.

This paper is organized as follows. Sample preparation and experimental details on the determination of film strain and of effective magnetoelastic coupling coefficients from stress measurements are introduced in Sec. II. The experimental results are presented in Sec. III. The experimental results are analyzed and discussed also in view of recent theoretical work in Sec. IV. The conclusion is given in Sec. V.

II. EXPERIMENTAL DETAILS

A. Sample preparation and experimental techniques

The experiments are performed in an ultrahigh vacuum chamber (UHV) with a base pressure of 5×10^{-11} mbar. Stress induced by film growth and by film magnetization is measured by the crystal curvature technique, which has been described in detail in Refs. 12, 29, and 30. Epitaxial layers of Fe, Co, and Ni are prepared by electron-beam (e-beam) evaporation under UHV conditions with a typical growth rate of 1 ML/min (1 ML: 1 monolayer=1 layer of atoms with the same surface density as compared to the substrate). The film thickness is calibrated by monitoring medium-energy electron diffraction (MEED) ($E=3$ keV) intensity oscillations[31] and by using a quartz microbalance. Surface structure and magnetism are studied *in situ* by low-energy electron diffraction (LEED) (Refs. 32–34) and magneto-optic Kerr effect (MOKE) (Ref. 35) measurements, respectively.

We use the Ir(100)-(1×1) surface as a substrate for film growth. The epitaxial misfit between Fe, Co, Ni, and this substrate induces considerable film strain, and the effect of strain on the magnetoelastic properties can be studied as discussed below.

The Ir(100) crystal (length: 12 mm, width: 2.5 mm, and thickness: 0.1 mm) is clamped at its top end along its width to a sample manipulator. The crystal is cleaned by Ar^+ ion bombardment (ion energy: 2 keV and ion current: 3 μA) and subsequent annealing at 1500 K for 10 s. This procedure leads to a clean front surface of the crystal, as checked by Auger electron spectroscopy (AES), which indicates that the surface contamination with foreign atoms such as C and O is below 1% of a monolayer. The backside of the crystal is not bombarded by ions, and it remains contaminated, rendering it inert for adsorption from the gas phase.[36]

The clean surface is characterized by a quasihexagonal (5×1)Hex reconstruction, as identified by LEED.[37] The Ir(100)-(5×1)Hex substrate is then annealed in oxygen ($P_{O_2}=5\times10^{-6}$ mbar) at 1400 K for 10 s until an oxygen terminated Ir(100)-(2×1)-O reconstruction is observed in LEED. The Ir(100)-(1×1) surface is finally obtained by subsequently exposing the Ir(100)-(2×1)-O layer to hydrogen ($P_{H_2}=2\times10^{-7}$ mbar at 400 K).[33,38] This preparation results in a Ir(100)-(1×1) surface, as checked by LEED, and this surface serves as a template for epitaxial growth of the magnetic layers. We note that the (5×1)-H reconstructed Ir(100) surface can be obtained by exposing the (5×1)Hex surface to 10 L H_2 at 300 K.

B. Determination of magnetoelastic coefficients and film strain from stress measurements

The dependence of the magnetic anisotropy on lattice strain is ascribed to the so-called magnetoelastic coupling.[21] Magnetoelastic coupling coefficients can be measured by either extracting the change in magnetic anisotropy of a sample upon straining it (e.g., by bending) or by measuring the magnetoelastic stress upon a magnetization reorientation in external magnetic fields.[12]

Magnetoelastic stress is the driving force for magnetostriction of bulk samples, and it reflects the correlation between lattice strain and magnetism, where it is experimentally found that a lattice of a magnetic material might expand or contract upon magnetization. For a bulk sample, a corresponding change in length is observed, where the resulting lattice strain is called magnetostriction. In a thin film however, a magnetization-induced strain of the film is not possible, as the film is bonded to a substrate, and a magnetoelastic stress evolves. This magnetoelastic stress will induce a curvature of a thin substrate, which is then measured by a cantilever crystal curvature technique. The magnetoelastic stress is then quantitatively extracted from the analysis of the magnetization-induced change in substrate curvature, and it is given by the corresponding magnetoelastic coupling coefficients.[12,39–42] The epitaxial misfit-induced lattice strain in a thin film can be as large as a several percent, and therefore the impact of strain on the magnetoelastic properties can be investigated over a larger strain range.

Another approach for measuring magnetoelastic coupling coefficients exploits the correlation between lattice strain and magnetic anisotropy, and it is based upon straining a sample by bending it. The resulting change in the magnetic anisotropy is extracted from the bending-induced change in a hard axis magnetization loop. This technique has been applied to amorphous alloys and metallic glasses, which were prepared in the form of a ribbon sample.[43,44] The maximum strain variation by bending is limited by the possibility of substrate breakage, and it is only of the order of 10^{-4} as the sample might break for larger strains.

All experimental investigations on magnetoelastic coupling by either technique indicate that the magnetoelastic coupling coefficients of nanometer thin films and at surfaces of bulk samples differ from the respective bulk values. Many results were obtained by the cantilever curvature technique applied to strained epitaxial films,[12,39,45–47] and some results are summarized in Ref. 13. It is found that the in-plane film strain modifies the magnetoelastic coupling. However, more measurements are required for a better understanding of the role of lattice strain for the modified magnetoelastic coupling. Here we present data on highly strained systems, where the epitaxial misfit-induced stress can be of the order of 10 GPa, as shown in Sec. II B 1 on film stress below.

The working principle of our stress measurement is based on an optical two-beam deflection technique. The stress-induced curvature of a thin single-crystal substrate is measured from the deflection of laser beams, which are reflected from the curved substrate onto position sensitive detectors.[29,30] We deposit the film material onto the front of the substrate, and the stress imbalance between the film-covered front surface and the back side of the substrate induces a change in substrate curvature, which is ascribed to the film stress.

We exploit two sources of stress, the epitaxial misfit-induced films stress τ_F and the magnetization-induced magnetoelastic stress τ_{ME}. The strength of this approach is that we can directly investigate the impact of misfit-induced film stress and strain on the magnetoelastic properties.

1. Film-growth-induced stress

An epitaxial misfit η gives rise to a film stress $\tau_F=\left(\frac{Y_F}{1-\nu_F}\right)\eta$, where the Young modulus Y and the Poisson ratio

TABLE I. Elastic constants c_{ij} (Ref. 48) and lattice constants a (Ref. 49). Young's modulus Y and Poisson's ratio ν are calculated from the elastic constants c_{ij} with $Y=(c_{11}+2c_{12})(c_{11}-c_{12})/(c_{11}+c_{12})$ and $\nu=c_{12}/(c_{11}+c_{12})$.

Element	c_{11} (GPa)	c_{12} (GPa)	c_{44} (GPa)	$Y/(1-\nu)$ (GPa)	a_F (Å)	a_S (Å)	η
bcc Fe	229	134	115	208	2.87		−0.053
fcc Fe[a]	200	134	77	154	3.574		+0.074
fcc Ni	249	152	118	215	3.52		+0.091
fcc Co	242	160	128	190	3.55		+0.082
fcc Ir	600	270	260	635		3.84	

[a]References 50 and 51.

ν of the film are given by Y_F and ν_F, respectively. The epitaxial misfit η is defined as $\eta=\frac{a_S-a_F}{a_F}$, where a_S and a_F denote the lattice constants of the substrate and film, respectively. Note that Y and ν are anisotropic in general, and the corresponding tensor transformations of the elastic properties need to be performed to account for the epitaxial orientation under investigation.[12,30]

We study cubic films with (100)-orientation, and here the ratio $Y_F/(1-\nu_F)$ is isotropic in the (100)-plane. The same holds true for the elastic properties of the substrate, which are calculated accordingly. Table I summarizes the respective values and the misfit η for the growth of fcc-Fe, bcc-Fe, fcc-Co, and fcc-Ni on Ir(100)-(1×1).

The stress in each layer of the film contributes to the stress-induced curvature $1/R$ of the substrate. The following relation gives the relation between film stress τ_F and curvature $1/R$,[12,30]

$$\tau_F t_F = \frac{Y_S t_S^2}{6(1-\nu_S)}\frac{1}{R},$$

where the substrate thickness is given by t_S, the film thickness by t_F and the subscripts F and S identify film and substrate properties, respectively. A constant film stress induces a curvature, which increases with film thickness. Thus, the slope of a plot $\tau_F t_F$ as a function of t_F gives the film stress τ_F.

Note, that epitaxial misfit induces a biaxial stress in general, and the analysis relies on a free two-dimensional curvature of the substrate even though the curvature is measured only along the length of the substrate. Near the clamping of the substrate its curvature along the width is hindered. Therefore, we use substrates with a large length-to-width ratio of 4–5, and this ensures a free two-dimensional bending near the bottom, free end of the substrate, where the measurements are taken. For length-to-width ratio smaller than 2, corrections need to be considered, which account for the influence of clamping.[12,52,53]

The epitaxial misfit remains constant during film growth until the critical thickness t_c of pseudomorphic growth is reached, and the misfit strain η relaxes. Thus, beyond pseudomorphic growth a smaller film strain ϵ is measured, and the film stress τ_F is reduced. Our measurements indicate the end of pseudomorphic growth around 10 ML for bcc Fe on Ir(100) and around 2 ML for Co and Ni on Ir(100). This difference is ascribed to the magnitude of epitaxial misfit, which is larger for Co and Ni, and smaller for bcc Fe (see Table I). A curvature measurement at a film thickness t_F beyond t_c reflects the average stress within the film.

The average film strain ϵ is calculated from $\epsilon=\frac{\Delta(\tau_F t_F)}{t_F}\frac{(1-\nu_F)}{Y_F}$, where $\Delta(\tau_F t_F)$ is the stress change measured between the beginning of growth at $t_F=0$ and the end of growth at t_F. This analysis is followed throughout this work to extract the average film strain ϵ from film stress-induced curvature measurement.

2. Magnetization-induced stress

A change in the magnetization direction of a sample along noncollinear directions induces a corresponding change in the magnetoelastic stress.[21] The resulting magnetostrictive change in length of a *bulk* sample was introduced above. The reorientation of the magnetization of a film, e.g., along two in-plane directions, induces a biaxial stress change, which gives rise to an anticlastic curvature of the film-substrate composite.[13] Thus, the measurement of the change in curvature upon a reorientation of the magnetization offers access to the effective magnetoelastic coefficients B_i^{eff}, as discussed in the literature.[12,54]

The magnetoelastic coupling coefficients B_1 and B_2 of a cubic material are determined from the magnetoelastic stress change upon a reorientation of the magnetization along orthogonal directions within the (100) plane. For the measurement of B_1, the magnetization M is aligned along [100] and [010] directions, and B_1 follows as $B_1=\tau^{M\|100}-\tau^{M\|010}$. Similarly, the values of B_2 are obtained by switching the magnetization direction from [110] to $[\bar{1}10]$, $B_2=\tau^{M\|110}-\tau^{M\|\bar{1}10}$. See Fig. 1 for an identification of directions within the Ir(100) surface.

Two Ir(100) substrates are used in the experiment to obtain both B_1 and B_2. One crystal has its length and width along Ir[100] and [010], the other along Ir[110] and $[\bar{1}10]$, respectively. For each determination of the effective B_i value, the magnetoelastic stress measurements are repeated at least three times, and the presented value is the average of these measurements. The error bar of B_i is given by the standard deviation of these measurements.

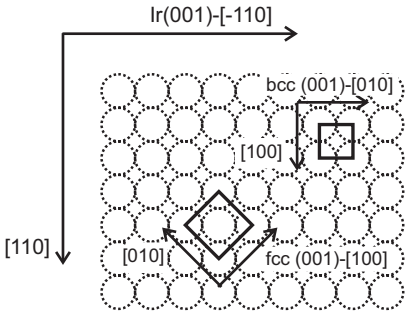

FIG. 1. The Ir(100) substrate and the respective directions of crystal axes in epitaxial films. The dashed circles represent Ir atoms at the surface. The solid squares indicate a square unit cell of epitaxial films of Fe, Co, and Ni, respectively.

III. RESULTS

A. Film stress and structure

The Ir(100)-substrate can be prepared with three different surface reconstructions, (1×1), (5×1)-H, and quasihexagonal (5×1)Hex. These surface structures have been studied by LEED, scanning tunnel microscope (STM), and other techniques.[37,57,58] We prepared these different surface structures to investigate the impact of the different surface reconstructions on stress and magnetic anisotropy of nanometer thin films.[59] We found some dependence on the different preparations on both stress state and magnetic properties. We show one example of the impact of the (5×1)-H vs the (1×1) structure on film stress in Fig. 2(c) and for the magnetoelastic stress of Fe in Fig. 3(a). The (5×1)-H surface leads to smaller film strain in thicker films >40 ML, as compared to the (1×1) surface.

In the following, we focus on the (1×1) surface as a template for subsequent growth of Fe, Ni, and Co. This preparation avoids possible additional complications due to the incorporation of Ir and H atoms into the film, which are expected for the (5×1)Hex and the (5×1)-H structures, respectively.

Figure 2 summarizes the stress change $\Delta(\tau_F t_F)$ measured during growth of Fe, Co, and Ni layers on Ir(100) at 300 K. The insets show an enlarged view of the stress change for the deposition of the first 3 ML. Panel (d) shows LEED pattern for Fe films of the indicated thickness, and the bottom panel shows a zoom-in to the (00) diffraction spot.

Figure 2(a) shows the stress due to Co growth on Ir(100)-(1×1). A tensile stress change is observed as the film thickness increases. Between 1 and 2 ML, the slope of the stress curve is almost constant, and it indicates a tensile film stress of +17 GPa. The stress relaxes after 2 ML and keeps increasing up to ≈40 ML, where the shutter of the evaporator has been closed. LEED measurements[59] for 2 ML Co show almost identical (1×1) patterns as compared to clean Ir(100), suggesting pseudomorphic growth. Extra spots emerge around the original spots in the (1×1) pattern for film thickness larger than 5 ML, suggesting the formation of misfit distortions.[55,56]

The stress curve for Ni growth on Ir(100)-(1×1) is shown in Fig. 2(b). Similarly to the stress results presented for Co on Ir(100), a large film stress of +15 GPa is observed from 1 to 2 ML. The stress relaxes for films thicker than 2 ML, and the film stress continues to increase up to the deposition of ≈40 ML. LEED measurements[59] show clear (1×1) patterns similar to that of the clean Ir(100)-(1×1) surface for a Ni thickness of up to 5 ML. The diffraction spots get blurred for films thicker than 5 ML.

The stress change during deposition of Fe on Ir(100)-(1×1) is shown in Fig. 2(c). Here, a tensile stress of +7 GPa is measured between 1–2 ML and then a compressive stress

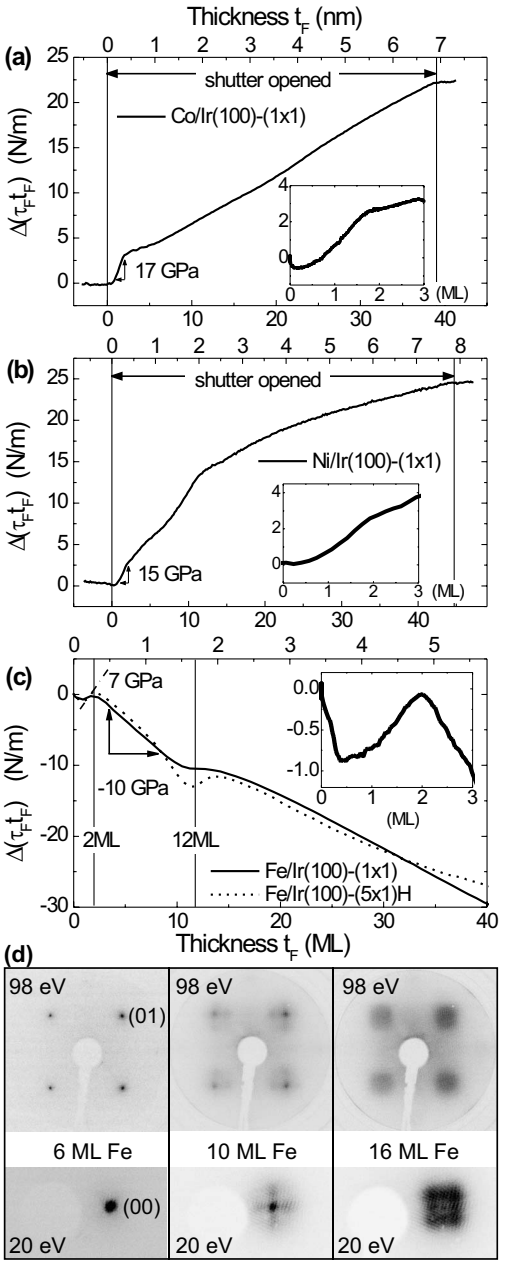

FIG. 2. Stress measurements for (a) Co on Ir(100)-(1×1), (b) Ni on Ir(100)-(1×1), and (c) Fe on different Ir(100) surface reconstructions. The insets show the stress change for the deposition of the first 3 ML. The LEED patterns of Fe on Ir(100) are shown in (d) for different Fe thicknesses at 98 eV. The small LEED panels for 20 eV indicate that the (00) spot splits for a thickness above 10 ML, identifying the formation of misfit dislocations (Refs. 55 and 56).

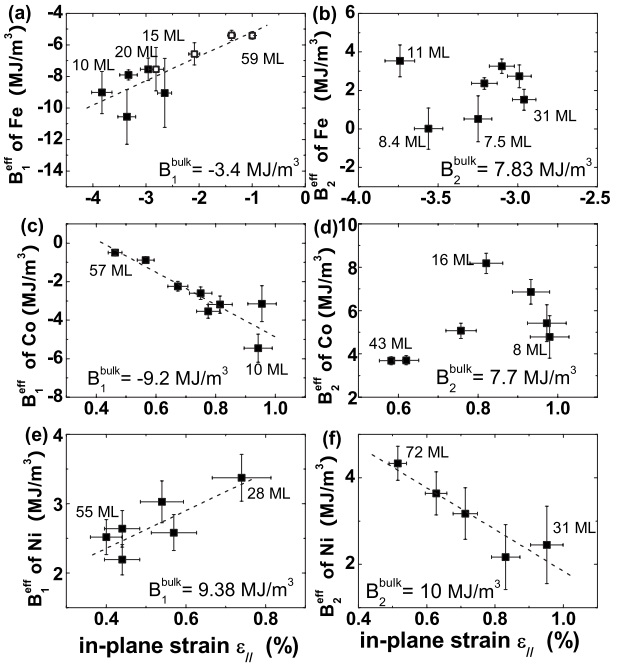

FIG. 3. Effective magnetoelastic coupling coefficients B_1 and B_2 of [(a) and (b)] Fe, [(c) and (d)] Co, and [(e) and (f)] Ni layers on Ir(100). The respective bulk values are given for comparison. The dashed lines are least-square linear fits to the data points. No such fitting is performed for (b) and (d). Open and closed symbols in (a) are for measurements on Ir(100)-(1×1) and (5×1)-H, respectively.

of −10 GPa is observed from 2–10 ML. The kink in the stress curve at 2 ML clearly marks the change in film stress from tensile to compressive. The film stress continues to change with a considerable slope up to the largest film thickness of 40 ML shown here.

LEED measurements of Fe/Ir(100) (Ref. 59) [Fig. 2(d)] show (1×1) patterns for $t_F \leq 10$ ML. With increasing film thickness beyond 10 ML, extra satellite spots appear[56] around the original spots, which were indicative for a 1×1 structure. From this we conclude that the critical thickness for pseudomorphic growth of Fe on Ir(100) is around 10 ML.

The insets of all stress curves indicate the stress change during the initial film growth up to 3 ML. All examples show that the stress curve up to the deposition of roughly 1 ML changes its slope continuously. In this low coverage regime, the change in surface stress of Ir upon coverage with the film material is essential, and this stress is not correlated with the epitaxial misfit.[60] Thus, a reduced slope, even a compressive stress for Fe, is observed.

B. Magnetoelastic coupling coefficients

The magnetoelastic coupling coefficients are obtained from magnetoelastic stress measurements for films of different thickness from a few monolayers up to about 10 nm (≈50 ML). The in-plane strain $\epsilon_{\|}$ is calculated from the averaged film stress as explained above. The experimentally determined effective magnetoelastic coupling coefficients B_1^{eff} and B_2^{eff} are presented in Fig. 3.

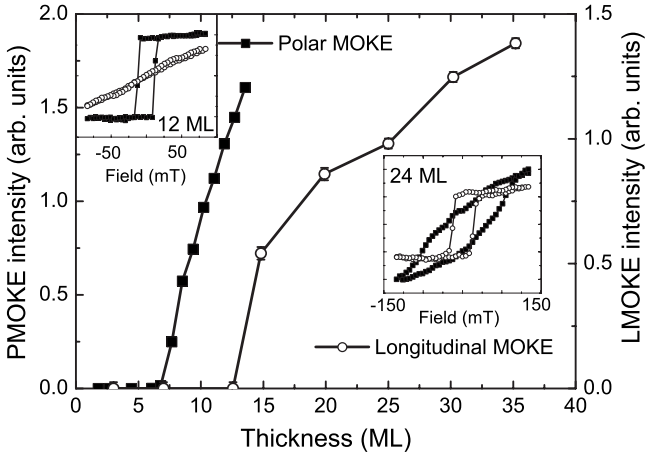

FIG. 4. MOKE intensity at remanence of Ni epitaxial layers on Ir(100)-(1×1) for different thickness. Filled and opened squares represent the results from MOKE measurements with polar and longitudinal geometries, respectively. Insets show the hysteresis loops of 12 and 24 ML Ni. All measurements were performed at 300 K. The in-plane field was oriented along Ni⟨100⟩, i.e., Ir⟨100⟩.

The data of Fig. 3 clearly indicate that the values of B_i^{eff} all differ from the respective bulk value, which is given in the plots for comparison. A linear strain dependence of B_i^{eff} offers a reasonable description in Figs. 3(a), 3(c), 3(e), and 3(f). The value of B_1^{eff} for Fe are measured on Ir(100) with (1×1) and (5×1)-H surface reconstructions, and the results are shown in Fig. 3(a) as the solid square and the open square, respectively. The data for B_2^{eff} of Fe and Co do not show a clear strain dependence; as shown in Figs. 3(b) and 3(d), the data show substantial scatter.

C. Magnetic anisotropy

MOKE measurements show hysteresis loops with full remanence for Fe layers with $t_F \geq 4$ ML and for Co layers with $t_F \geq 2$ ML. We have not observed magnetic hysteresis curves in Fe films thinner than 4 ML and in Co films thinner than 2 ML even at a lower temperature of 180 K. These results reveal that the easy axis of magnetization is in plane for Fe ($t \geq 4$ ML) and Co ($t \geq 2$ ML) on Ir(100).

The magnetic anisotropy is different for Ni on Ir(100). As shown in the inset of Fig. 4, squarelike hysteresis loops are observed by polar MOKE measurements for Ni with $7 \leq t_F < 15$ ML, indicating an out-of-plane easy magnetization axis. Above 15 ML, longitudinal MOKE measurements show squarelike hysteresis loops along Ni⟨100⟩ and ⟨110⟩, whereas the polar MOKE measurements do not indicate an easy axis loop. These results reveal that the easy magnetization direction changes from out of plane to in plane with increasing film thickness around 15 ML.

IV. DISCUSSION

A. Structure and film strains from stress and LEED measurements

According to linear elasticity theory, the film stress τ_F during pseudomorphic growth is proportional to the misfit η

between film and substrate, and it is given by $\tau_F=(\frac{Y}{1-\nu})_F\eta$.[12] Therefore stress measurements can be exploited to deduce pseudomorphic misfit strain η and film strain ϵ from respective stress measurements in the pseudomorphic regime and beyond, respectively. Beyond pseudomorphic growth, the stress analysis gives an average in-plane strain $\epsilon_\parallel$ of the film. By combining stress and LEED measurements, we can quantitatively analyze the lattice strain of monolayers.

For Fe on Ir(100), the misfit between the in-plane lattice spacing of bcc-Fe and Ir(100) is −5.3%, between fcc-Fe and Ir(100) it is +7.4%. As a result, a compressive film stress of $\tau_F=-11$ GPa is expected for bcc-Fe, and a tensile stress of $\tau_F=+11.4$ GPa is expected for fcc-Fe on Ir(100).

As shown in Fig. 2(c), we observe large compressive stress of −10 GPa from 2 up to 10 ML, and this is ascribed to the misfit between bcc-Fe and Ir(100). The tensile stress of +7 GPa between 1 and 2 ML is ascribed to the growth of a fcc-Fe precursor. A bcc Fe film grows on its top for $t_F>2$ ML. This scenario is supported by a quantitative LEED study.[61] Both the relaxed film stress and the extra diffraction spots in the LEED pattern[61] indicate that a dislocation network is formed for the deposition of more than 10 ML Fe. The pseudomorphic growth of bcc-Fe ends at 10 ML.

For Co and Ni on Ir(100), the large film stress of +17 and +15 GPa between 1 and 2 ML is ascribed to the misfit-induced stress of pseudomorphically strained fcc-Co and fcc-Ni films on Ir(100), respectively. For both fcc-Co and fcc-Ni pseudomorphic growth ends at 2 ML. Beyond the end of pseudomorphic growth, the film stress continues to change with increasing film thickness.

The most important conclusion from the stress measurements is that the magnitude of film strain remains sizable with a magnitude in the high subpercent range even for a thickness beyond pseudomorphic growth. Beyond pseudomorphic growth diffraction experiments such as LEED indicate extra spots, which are ascribed to the formation of misfit dislocations.[61] However the observation of diffraction patterns which are due to misfit dislocations does by no means imply that the film strain drops to zero once misfit dislocations are formed.

Our stress results also disagree with the strain prediction of a simple coincidence lattice approach,[62] which has been proposed to tackle film strain beyond pseudomorphic growth. Such a model suggests a considerably reduced average film strain, often by an order of magnitude, which is in contrast to the large stress which we measure beyond pseudomorphic growth. To obtain a more efficient strain relaxation, compared to what we observe for deposition on Ir(100) at 300 K, thermal annealing of the film structure might be called for. We refrained from doing this to avoid potential intermixing at the film-substrate interface, which would render the analysis of the data more troublesome due to the resulting inhomogeneous elemental composition.

Our stress measurements identify a residual film strain of up to 1% even in nanometer thick films. This residual film strain has an important impact on the magnetoelastic coupling, as discussed below.

B. Strain-dependent magnetoelastic coupling

The compilation of our experimental data on the effective magnetoelastic coupling B_i^{eff} in Fig. 3 clearly shows that in all examples B_i^{eff} deviates strongly from the respective bulk value. As indicated in Fig. 3(a), for Fe films with different thickness (20 ML as compared to 15 ML) but similar film strain, the values of B_1^{eff} are alike. This implies that the magnetolastic coupling coefficient B_1^{eff} is strain dependent rather than thickness dependent.

Our result of a strain-dependent magnetoelastic coupling has important implications for the understanding of the magnetic anisotropy of epitaxial monolayers, and this aspect will be discussed below for the spin-reorientation transition (SRT) of Ni on Ir(100). Here we present our analysis of the deviation of B_i^{eff} from its bulk value.

Magnetoelastic coupling coefficients, which differ from the bulk value have been reported before.[12,39,44,63–66] The common characteristic of these works was that either a thin film ($t_F\approx$ nanometer range) or a surface sensitive measurement technique[44] had been used.

Thus, the first description of the unexpected behavior of B_i^{eff} was discussed in view of a so-called surface effect, where a deviation of $B_i^{\text{eff}}(t_F)=B_{\text{bulk}}+\text{const}/t_F$ has been proposed. This view suggests that B_i^{eff} approaches the bulk value with increasing film thickness. However, later experimental work has provided clear evidence that this approach is not valid. For example films of the same thickness but different stress have been prepared and their magnetoelastic coupling has been measured to be different.[39] These results indicate different B_i^{eff} for the same film thickness, disqualifying the general applicability of a so-called surface effect. In contrast, these results indicate the decisive role of strain.

The effect of lattice strain on the magnetoelastic coupling has been identified as an important contribution to B_i^{eff}.[64,66–69] Thus, whenever the lattice strain ϵ changes, so does B_i^{eff}, i.e., $B_i^{\text{eff}}=B_i^{\text{eff}}(\epsilon)$. Previous works and the present study do suggest that the strain model $B_i^{\text{eff}}(\epsilon)$ may give a reasonable description of the experimental results. Note however, that a clear cut experimental discrimination between both models, $B_i^{\text{eff}}(t_F)$ vs $B_i^{\text{eff}}(\epsilon)$ might be disguised by the thickness dependence of lattice strain.[13] However, a variation in lattice strain in proportion to $1/t_F$ cannot be confirmed experimentally, and a more complicated relation between ϵ and t_F has been proposed.[13]

In Fig. 3 the values of B_i^{eff} are plotted as a function of the average film strain $\epsilon_\parallel$. The strain dependence of B_i^{eff} is described by $B_i^{\text{eff}}(\epsilon)=B_i+D_i\epsilon_\parallel$. The dashed lines in Fig. 3 reveal that in some cases this approach gives a reasonable description of the experimental data. This description of the experimental results support the idea of a strain-dependent magnetoelastic coupling. Also *ab initio* calculations support this view, and a strain dependence of the magnetoelastic coupling has been explicitly proposed.[70–75]

The compilation of our results of B_i^{eff} in Fig. 3 indicates that the following relations give a reasonable fit of the experimental data in terms of $B_i^{\text{eff}}(\epsilon_\parallel)$, where $\epsilon_\parallel$ is the average in-plane strain of the film:

(a) bcc-Fe with negative film strain,

$$B_1^{\text{eff}}=-3.6(\pm 1.0)\ \frac{\text{MJ}}{\text{m}^3}+155(\pm 37)\ \frac{\text{MJ}}{\text{m}^3}\times\epsilon_\parallel,$$

(b) fcc-Co with positive film strain,

$$B_1^{\mathrm{eff}} = 3.5(\pm 0.7)\ \frac{\mathrm{MJ}}{\mathrm{m}^3} - 842(\pm 126)\ \frac{\mathrm{MJ}}{\mathrm{m}^3} \times \epsilon_{\parallel},$$

[(c) and (d)] fcc-Ni with positive film strain,

$$B_1^{\mathrm{eff}} = 1.3(\pm 1.0)\ \frac{\mathrm{MJ}}{\mathrm{m}^3} + 273(\pm 197)\ \frac{\mathrm{MJ}}{\mathrm{m}^3} \times \epsilon_{\parallel},$$

$$B_2^{\mathrm{eff}} = 6.6(\pm 1.0)\ \frac{\mathrm{MJ}}{\mathrm{m}^3} - 408(\pm 107)\ \frac{\mathrm{MJ}}{\mathrm{m}^3} \times \epsilon_{\parallel}.$$

In this study we fitted all the data obtained by ME stress measurements without forcing the bulk value for zero strain. We acknowledge that a linear fitting of the strain dependent $B_i^{\mathrm{eff}} = B_i + D_i \epsilon$ considers only first-order and second-order strain terms in the expression of the magnetic anisotropy, and higher-order terms may also play an important role.[72] The values of B_i and D_i are obtained from least-square fitting of the experimentally determined B_i^{eff} and $\epsilon_{\parallel}$.

We refrain from fitting a linear function to the data points for B_2^{eff} of Fe and Co in Figs. 3(b) and 3(d). We judge that the scatter of these data points does not justify this. We note that for B_2 of Co and Fe also the surface effect model $B_2^{\mathrm{eff}}(t_F)$ does not give a valid description, and we remark that for both cases the measured values deviate sharply from the published bulk values, as indicated in Fig. 3. It remains an open question whether the data of B_2 of Co and Fe should be rather described with higher-order strain contributions. In view of the experimental error bars we do not follow this approach here.

C. Nonlinear magnetoelastic coupling: Experimental results in comparison with theoretical predictions

Before comparing our results to those of the theory, we elucidate important aspects in the description of our results in view of a theoretical analysis, which acknowledges the symmetry of the underlying expressions fully.

Our experimental results on a linear strain dependence of $B^{\mathrm{eff}}(\epsilon) = B + D\epsilon_{\parallel}$ gives rise to a magnetoelastic anisotropy contribution to the magnetic anisotropy in proportion to $B^{\mathrm{eff}}(\epsilon)\epsilon_{ij}$, i.e., second-order in strain. This leads to the expression nonlinear magnetoelastic coupling, which we use here.

The magnetoelastic (ME) energy density can be expanded as a function of higher-order strain contributions as $f_{\mathrm{ME}} = f_{\mathrm{ME}}^{(1)} + f_{\mathrm{ME}}^{(2)} + \ldots$, in which the superscript refers to the order of strain contributions. The justification of this expansion is given in Ref. 40 based on a phenomenological theory of nonlinear magnetoelasticity. It is simplified by limiting the expansion to the quadratic harmonic polynomials in α_i:[73]

$$f_{\mathrm{ME}}^{(1)} = B_1(\epsilon_{11}\alpha_1^2 + \epsilon_{22}\alpha_2^2 + \epsilon_{33}\alpha_3^2) + 2B_2(\epsilon_{12}\alpha_1\alpha_2 + \epsilon_{23}\alpha_2\alpha_3 + \epsilon_{31}\alpha_3\alpha_1), \quad (1)$$

$$f_{\mathrm{ME}}^{(2)} = \frac{1}{2}(B_1 + m_1^{\gamma,2})(\epsilon_{11}^2\alpha_1^2 + \epsilon_{22}^2\alpha_2^2 + \epsilon_{33}^2\alpha_3^2) + \frac{1}{2}m_2^{\gamma,2}(\epsilon_{11}\epsilon_{22}\alpha_3^2 + \mathrm{cycl.}) + \frac{1}{2}(m_3^{\gamma,2} - B_1)(\epsilon_{12}^2\alpha_3^2 + \mathrm{cycl.}) + m_1^{\epsilon,2}(\epsilon_{11}\epsilon_{23}\alpha_2\alpha_3 + \mathrm{cycl.}) + (B_2 + m_2^{\epsilon,2})[(\epsilon_{11} + \epsilon_{22})\epsilon_{12}\alpha_1\alpha_2 + \mathrm{cycl.}] + (B_2 + m_3^{\epsilon,2})(\epsilon_{12}\epsilon_{23}\alpha_1\alpha_3 + \mathrm{cycl.}). \quad (2)$$

In these expressions B_1 and B_2 are the first-order ME coefficients. $m_1^{\gamma,2}$, $m_2^{\gamma,2}$, $m_1^{\epsilon,2}$, $m_2^{\epsilon,2}$, $m_3^{\gamma,2}$, and $m_3^{\epsilon,2}$ are the second-order ME coefficients. $m_1^{\gamma,2}$ and $m_2^{\gamma,2}$ are related to pure tensile strains, $m_1^{\epsilon,2}$ and $m_2^{\epsilon,2}$ are related to tensile and shear strains, and $m_3^{\gamma,2}$ and $m_3^{\epsilon,2}$ are related to pure shear strain.

In the magnetoelastic stress measurements, the magnetization is switched between certain directions, and the magnetoelastic-coupling-induced stress change during the process is related to the ME coefficients according to the geometry of the measurement. Theory suggests six geometries which allow us to extract the ME coefficients from ME stress measurements.[73]

In practice, the available geometries of ME stress measurements are often limited by the external magnets, i.e., by the geometry and strength of the magnetic fields. For example, the magnetic field is normally applied along two orthogonal directions, and it may occur that one direction is a hard magnetization axis, and the magnetization cannot be saturated along that direction. Therefore it is very difficult to perform ME stress measurements along all proposed geometries.

In view of this experimental constraint, our measurements of effective ME coefficients B_i^{eff} do not give directly the second-order ME coefficients as defined above but a combination thereof with first-order ME coefficients and elastic constants. According to the geometry of the ME stress measurements of this work, the expression of B_i^{eff} in terms of the magnetoelastic coefficients in Eq. (2) is as follows:

$$B_1^{\mathrm{eff}} = B_1 + D_1\epsilon_{\parallel}, D_1 = B_1 + m_1^{\gamma,2} + \frac{c_{12}}{c_{11}}m_2^{\gamma,2},$$

$$B_2^{\mathrm{eff}}(\epsilon) = B_2 + 2D_2\epsilon_{\parallel}, D_2 = \frac{1}{2}\left[(B_2 + m_2^{\epsilon,2}) - \frac{c_{12}}{c_{11}}m_1^{\epsilon,2}\right].$$

Here the in-plane film strain is $\epsilon_{11} = \epsilon_{22} = \epsilon_{\parallel}$, and the out-of-plane strain follows as $\epsilon_{\perp} = -2\frac{c_{12}}{c_{11}}\epsilon_{\parallel}$.

Together with Eqs. (1) and (2), the relation between magnetoelastic energy and film strain is given by a parabolic expression, where both first-order and second-order strain contributions enter. Higher-order contributions in strain may lead to more complicated curves,[22,72] and also a nonmonotonic dependence of the magnetic anisotropy on strain may result.

Table II lists the compilation of both experimental and theoretical values. We include also previous experimental data[12,45,66] on cubic systems. A measurement of hcp-Co on

TABLE II. Theoretical [adapted from *ab initio* calculations (Refs. 23 and 72)] and experimental results of magnetoelastic coupling coefficients B_i and the nonlinear strain-dependent D_i. (All values are given in MJ/m^3.) LSDA: local spin-density approximation and GGA: generalized gradient approximation.

		B_1	D_1	B_2	$2D_2$
fcc Co	LSDA[a]	−15.9	212	3	58
	GGA[a]	−9.8	186	4.5	−71
	Expt.[b],[c]	−9.2		7.7	
	Co/Ir(100)	3.5	−842	1.8	930
fcc Ni	LSDA[a]	12.6	−103	16.9	−132
	GGA[a]	10.2	−53	11.1	−47
	Ni/Cu(100)[d],[e]	9.4	−234	10	
	Ni/Ir(100)	1.3	273	6.6	−408
bcc Fe	LSDA[a]	−10.1	337	−7.0	−40
	GGA[a]	−2.4	383	−3.9	18
	Fe/MgO(100), Fe/Cr/MgO(100)[f],[g]	−3.4	1100	7.8	−365
	Fe/Ir(100)[h]	−3.6	155		

[a]References 23 and 72.
[b]The experimental values of the first-order ME coefficients B_1 and B_2 of fcc Co are calculated from the magnetostriction constants λ_{100} and λ_{111}, which were extrapolated from measurements on PdCo alloys, from Ref. 12.
[c]Reference 12.
[d]Experimental data B_1 and D_1 of fcc Ni are from Ref. 66 for Ni/Cu(100) with positive film strain.
[e]Reference 66.
[f]The experimental data B_1, B_2, D_1, and D_2 of Fe are from Ref. 45 for Fe(001)/MgO(001) and Fe/Cr/MgO(001) with positive film strain, in which the Fe films are deposited at different temperature to obtain different film strain.
[g]Reference 45.
[h]B_2^{eff} of bcc-Fe has been measured, see Fig. 3(b), but the scatter of the data does not allow for a description in terms of $B_2=B_2(\epsilon)$.

W(100) has been described in literature, and the results for B_4 are presented in Ref. 64.

The visual inspection of Table II shows that a quantitative agreement between theory and experiment is not observed for any result. Note, that different calculation schemes, local spin-density approximation (LSDA) and generalized gradient approximation (GGA), produce different results. Also, experimental data of the same element vary between the present results on Ir as compared to previous work.

To appreciate the disagreement between the data it is important to acknowledge that also the consideration of the experimental error bars for all values, as presented above, does not change the result of an overall poor agreement.

The disagreement between experiment and theory for B_2 of unstrained bulk Fe has been discussed before,[73] and it has been concluded that the calculation methods are inherently flawed for the calculation of the magnetoelastic properties of Fe. This remark illustrates clearly the difficulty of an *ab initio* based calculation of magnetoelastic effects.

We may speculate about the origin of the discrepancy between all data, and we may suggest that the description of the impact of strain on the magnetoelastic coupling *cannot* be described in view of a simple linear strain correction over a wide range of strain. This speculation might be corroborated by the results on bcc Fe.

Comparing B_1 and D_1 for bcc-Fe with negative strain ($\epsilon_\parallel$ between −1% and −4%) to the previous experimental results for bcc-Fe under positive strain, one finds that the values of B_1 are almost the same, while D_1 is quite different for both strain situations. This might suggest that the strain dependence of B_i is not the same for positive and negative strains, which is in line with a nonmonotonic dependence of magnetic anisotropy on the lattice distortion. Tentatively, we may ascribe this to higher-order strain contributions to the magnetic anisotropy. The inclusion of higher-order strain contributions could also account for the opposite sign of D_1 for fcc-Ni on Cu(100) (Ref. 66) (high strain, $\epsilon_\parallel$ between 1%–2.5%) and Ir(100) (this study, low strain, $\epsilon_\parallel \sim 0.4\%-0.7\%$).

A further issue could be related to our derivation of film strain from film stress. Our analysis of the average film strain as derived from the stress measurements neglects a possible spatial variation in strain throughout the film volume. Due to the lack of a more sophisticated strain analysis, we assume a proportionality between stress and strain. It has been proved by previous experiments that this treatment works well for ultrathin films of a few monolayers,[12] but it may be questionable at higher film thickness. An illustration of the shortcoming of a simple strain analysis might be indicated for B_2^{eff} of fcc-Co on Ir(100) [Fig. 3(d)], which might suggest a different strain dependence for a film thickness below and above 20 ML.

We conclude this section with the important and clear conclusion that all experimental results and calculations indicate that even a small strain in the subpercent range can

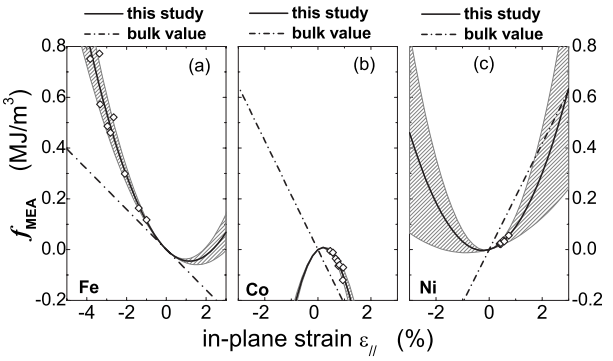

FIG. 5. Magnetoelastic anisotropy for an out-of-plane magnetization direction of Fe(001), Co(001), and Ni(001) films. The hollow dots are calculated directly from the magnetoelastic stress measurements; the solid curve is from the linear fitting of B_1^{eff} as given in equations (a)–(d), and the uncertainty caused by the error bar indicated in parentheses in equations (a)–(d) is shown as the shaded area. The boarder of the shaded area is from the curve with the extreme conditions. The dash-dot line is calculated with the bulk value, i.e., a constant magnetoelastic coupling, giving rise to a linear magnetoelastic anisotropy contribution.

modify the magnetoelastic coupling significantly. This statement remains valid irrespective of a conclusive theoretical description of all results.

D. Nonlinear magnetoelastic coupling and its impact on the magnetic anisotropy

The magnetoelastic anisotropy is often a decisive contribution to the magnetic anisotropy of epitaxially strained films.[12,13] The magnetoelastic anisotropy is used to calculate the difference in energy density between an out-of-plane magnetization and an in-plane magnetization.

Both magnetization directions give rise to different magnetoelastic anisotropies, as the film is tetragonally distorted with different strains in plane as compared to out of plane. For strained (100) cubic films the magnetoelastic contribution is calculated from $f_{\text{ME}}=B_1^{\text{eff}}(\epsilon_{\parallel}-\epsilon_{\perp})$. Accordingly, a positive f_{ME} favors an easy axis out of plane, and a negative f_{ME} favors an in-plane easy magnetization direction. The strain-dependent magnetoelastic anisotropy curves of Fe, Co, and Ni films are shown in Fig. 5. They are calculated using B_1^{eff} from our experimental values, and the bulk behavior of a constant B_1^{eff} is shown for comparison.

As shown in Fig. 5, our study indicates that the positive value of the magnetoelastic anisotropy for bcc-Fe(001) and fcc-Ni(001) films favors an out-of-plane orientation of the easy magnetization direction. Whether an out-of-plane easy magnetization direction is observed depends on the magnitude of the stray field energy, which acts against a polar magnetization. Its contribution is decisive for Fe, and the easy magnetization direction is in plane. However, for Ni both contributions can cancel, and an out-plane magnetization is observed, as discussed below. For fcc-Co(001) films the magnetoelastic anisotropy energy is always negative, and this favors an in-plane easy axis, which is observed in our experiments.

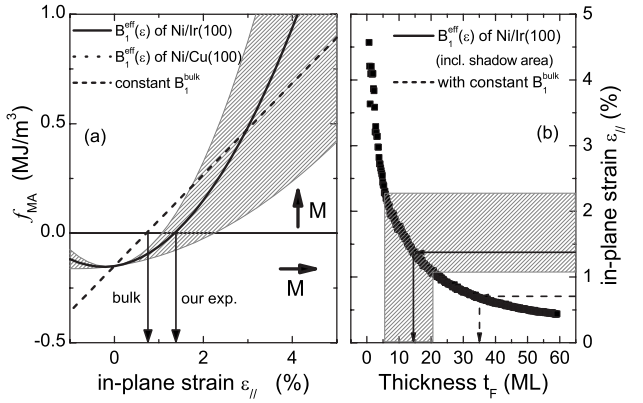

FIG. 6. Magnetic anisotropy energy ($f_{\text{MA}}=f_{\rightarrow}-f_{\uparrow}$) and the in-plane strain from stress measurement for Ni monolayers on Ir(100). The magnetic anisotropy is calculated considering shape (using M_S of bulk Ni) and magnetoelastic anisotropies. The solid curve shows the magnetic anisotropy with strain-dependent B_1^{eff} obtained from our experimental results, and the dashed line is calculated with a constant bulk value of B_1 for comparison. Accordingly, the film strain and thickness where a spin reorientation may occur is marked by arrows. The uncertainty caused by the error bar in the linear fitting of $B_i^{\text{eff}}(\epsilon)$ is indicated as the shaded area.

The magnetic anisotropy energy density f_{MA} is given by $f_{\text{MA}}=f_{\text{ME}}-\frac{1}{2}\mu_0 M_S^2$, where the last term reflects the stray field energy density, which favors an in-plane magnetization direction [saturation magnetizations of: fcc-Co (Refs. 76 and 77), $M_S=1447$ kAm^{-1} and $\frac{1}{2}\mu_0 M_S^2=1.32$ MJ/m^3; fcc-Ni (Ref. 77), $M_S=493$ kAm^{-1} and $\frac{1}{2}\mu_0 M_S^2=0.15$ MJ/m^3; bcc-Fe (Ref. 77), $M_S=1717$ kAm^{-1} and $\frac{1}{2}\mu_0 M_S^2=1.85$ MJ/m^3]. Here

$$f_{\text{MA}}=B_1^{\text{eff}}(\epsilon_{\parallel}-\epsilon_{\perp})-\frac{1}{2}\mu_0 M_S^2.$$

We replace B_1^{eff} with the expression given in Sec. IV C, and we obtain a parabolic plot of f_{MA} as a function of in-plane strain $\epsilon_{\parallel}$ presented in Fig. 6(a). This approach is followed to discuss the spin reorientation transition in Ni/Ir(100), see Fig. 4.

The calculated magnetic anisotropy energy of Ni on Ir(100) is plotted in Fig. 6(a), and the in-plane strain as a function of thickness is shown in Fig. 6(b). The strain-dependent magnetoelastic coefficient B_1^{eff} of Ni on Ir(100) leads to a strain-dependent magnetic anisotropy as shown in Fig. 6(a) (solid curve).

The estimation of f_{MA} using a constant bulk value of B_1 is also shown as the dashed line for comparison. The intersections of the curves with the line of f_{MA} indicate the critical film strain where a spin reorientation is expected. The solid curve of f_{MA} with the experimental value of B_1^{eff} shows that as the film strain increases beyond 1.4%, f_{MA} changes from negative to positive and the easy magnetization direction changes from in plane to out of plane. In contrast, the bulk value B_1^{bulk} leads to a critical film strain of $\epsilon_{\parallel}\sim 0.7\%$. The thickness dependence of the in-plane strain as shown in Fig. 6(b) indicates that the film strain decreases as the film thick-

ness increases. Combining the data from Figs. 6(a) and 6(b) tells us that the constant bulk value of B_1^{bulk} forces the spin reorientation at t_F=35 ML, in contrast to the experimental observation.

However, the experimentally determined value of B_1^{eff} gives a spin reorientation at about t_F=15 ML, in good agreement with the experimental observation. The error bar of the B_1^{eff} from magnetoelastic stress measurement is also taken into account causing the uncertainty of f_{MA} and t_F where a spin reorientation may happen, and it is shown as the shaded area in Fig. 6. We conclude that only the consideration of a nonbulklike B_i^{eff} gives a proper description of the thickness dependence of the SRT. This agreement between estimated and experimentally observed thickness of the SRT supports the concept of a strain-induced change in the magnetoelastic coupling coefficient B_1^{eff}.

Similarly, the magnetic anisotropies are also estimated for Fe and Co on Ir(100) with both the experimentally determined B_1^{eff} and bulk values of B_1^{bulk}. Here, the balance of the magnetic anisotropy energy density shows an in-plane easy magnetization direction in the thickness range we studied for both Fe and Co. These results are consistent with our MOKE measurements, which indicate an in-plane easy magnetization.[59]

V. CONCLUSIONS

Direct measurements of the magnetoelastic coupling coefficients of epitaxial monolayers reveal nonbulklike magnetoelastic couplings in Fe, Co, and Ni epitaxial layers on Ir(100). The combination of film stress and magnetoelastic stress measurements reveals that lattice strain, even in the subpercent level, may change the magnetoelastic coupling considerably. Thus, a reliable discussion of the magnetic anisotropy of strained monolayers needs to consider the effective magnetoelastic coefficients. Reference to bulk magnetoelastic coefficients may produce erroneous results.

The application of the effective magnetoelastic coefficients lead to a proper description of spin reorientation transitions in strained monolayers. Our experimental results broaden the scarce database of magnetoelastic coupling coefficients, and they may serve as a comparison for recent and future calculations of magnetoelastic properties. At present, the agreement between theory and experiments is unsatisfactory and more work is called for.

[1] U. Gradmann, in *Handbook of Magnetic Materials* (Elsevier Science, New York, 1993), Chap. 1, pp. 1–96.
[2] B. Heinrich, Z. Celinski, J. F. Cochran, A. S. Arrott, and K. Myrtle, J. Appl. Phys. **70**, 5769 (1991).
[3] P. Bruno, *Magnetismus von Festkörpern und Grenzflächen*, Lecture Notes (Forschungszentrum Jülich, Jülich, Germany, 1993).
[4] K. Baberschke, M. Donath, and W. Nolting, *Band Ferromagnetism* (Springer-Verlage, Berlin, 2001).
[5] R. Skomski, J. Phys.: Condens. Matter **15**, R841 (2003).
[6] S. D. Bader, Surf. Sci. **500**, 172 (2002).
[7] P. Bruno and J.-P. Renard, Appl. Phys. A: Solids Surf. **49**, 1833 (1989).
[8] D. L. Mills, in *Ultrathin Magnetic structures* (Springer, New York, 1994), Chap. 3, pp. 92–1211.
[9] R. Wu, L. Chen, and A. J. Freeman, J. Appl. Phys. **81**, 4417 (1997).
[10] M. Farle, W. Platow, A. N. Anisimov, P. Poulopoulos, and K. Baberschke, Phys. Rev. B **56**, 5100 (1997).
[11] F. El Gabaly, S. Gallego, C. Munoz, L. Szunyogh, P. Weinberger, C. Klein, A. K. Schmid, K. F. McCarty, and J. de la Figuera, Phys. Rev. Lett. **96**, 147202 (2006).
[12] D. Sander, Rep. Prog. Phys. **62**, 809 (1999).
[13] D. Sander, J. Phys.: Condens. Matter **16**, R603 (2004).
[14] C. A. F. Vaz, J. A. C. Bland, and G. Lauhoff, Rep. Prog. Phys. **71**, 056501 (2008).
[15] J. Dorantes-Dávila and G. M. Pastor, Phys. Rev. B **72**, 085427 (2005).
[16] A. Murayama, K. Hyomi, J. Eickmann, and C. M. Falco, Phys. Rev. B **60**, 15245 (1999).
[17] C. A. F. Vaz and J. A. C. Bland, Phys. Rev. B **61**, 3098 (2000).
[18] J. Wenisch, C. Gould, L. Ebel, J. Storz, K. Pappert, M. J. Schmidt, C. Kumpf, G. Schmidt, K. Brunner, and L. W. Molenkamp, Phys. Rev. Lett. **99**, 077201 (2007).
[19] S. Boukari, E. Beaurepaire, H. Bulou, B. Carrière, J. P. Deville, F. Scheurer, M. DeSantis, and R. Baudoing-Savois, Phys. Rev. B **64**, 144431 (2001).
[20] J. Prokop, D. A. Valdaitsev, A. Kukunin, M. Pratzer, G. Schönhense, and H. J. Elmers, Phys. Rev. B **70**, 184423 (2004).
[21] C. Kittel, Rev. Mod. Phys. **21**, 541 (1949).
[22] T. Burkert, O. Eriksson, P. James, S. I. Simak, B. Johansson, and L. Nordström, Phys. Rev. B **69**, 104426 (2004).
[23] M. Fähnle and M. Komelj, Z. Metallkd. **93**, 970 (2002).
[24] R. Wu, L. Chen, and A. J. Freeman, J. Magn. Magn. Mater. **170**, 103 (1997).
[25] R. Wu, Z. Yang, and J. Hong, J. Phys.: Condens. Matter **15**, S587 (2003).
[26] R. Q. Wu, L. J. Chen, A. Schick, and A. J. Freeman, J. Magn. Magn. Mater. **177-181**, 1216 (1998).
[27] T. Burkert, L. Nordström, O. Eriksson, and O. Heinonen, Phys. Rev. Lett. **93**, 027203 (2004).
[28] D. Sander, W. Pan, S. Ouazi, J. Kirschner, W. Meyer, M. Krause, S. Müller, L. Hammer, and K. Heinz, Phys. Rev. Lett. **93**, 247203 (2004).
[29] D. Sander and J. Kirschner, Appl. Phys. A: Mater. Sci. Process. **87**, 419 (2007).
[30] D. Sander, Z. Tian, and J. Kirschner, Sensors **8**, 4466 (2008).
[31] D. Sander, S. Ouazi, V. S. Stepanyuk, D. I. Bazhanov, and J. Kirschner, Surf. Sci. **512**, 281 (2002).
[32] K. Heinz, Prog. Surf. Sci. **27**, 239 (1988).
[33] K. Heinz, G. Schmidt, L. Hammer, and K. Müller, Phys. Rev. B **32**, 6214 (1985).
[34] H. C. Poon, D. K. Saldin, D. Lerch, W. Meier, A. Schmidt, A. Klein, S. Müller, L. Hammer, and K. Heinz, Phys. Rev. B **74**, 125413 (2006).

[35] S. D. Bader, J. Magn. Magn. Mater. **100**, 440 (1991).
[36] D. Sander, U. Linke, and H. Ibach, Surf. Sci. **272**, 318 (1992).
[37] A. Schmidt, W. Meier, L. Hammer, and K. Heinz, J. Phys.: Condens. Matter **14**, 12353 (2002).
[38] T. Ali, B. Klötzer, A. V. Walker, Q. Ge, and D. A. King, J. Chem. Phys. **109**, 9967 (1998).
[39] M. Weber, R. Koch, and K. H. Rieder, Phys. Rev. Lett. **73**, 1166 (1994).
[40] E. du Trémolet de Lacheisserie, *Magnetostriction Theory and Applications of Magnetoelasticity* (CRC, Boca Raton, FL, 1993).
[41] A. Tam and H. Schroeder, J. Appl. Phys. **64**, 5422 (1988).
[42] J. Wetz, E. du Trémolet de Lacheisserie, and L. T. Baczewski, Appl. Phys. Lett. **68**, 132 (1995).
[43] J. M. Barandiarán, A. Hernando, V. Madurga, O. V. Nielsen, M. Vázquez, and M. Vázquez-López, Phys. Rev. B **35**, 5066 (1987).
[44] S. W. Sun and R. C. O'Handley, Phys. Rev. Lett. **66**, 2798 (1991).
[45] G. Wedler, J. Walz, A. Greuer, and R. Koch, Phys. Rev. B **60**, R11313 (1999).
[46] M. Ciria, J. I. Arnaudas, L. Benito, C. de la Fuente, A. del Moral, K. Ha, and R. C. O'Handley, Phys. Rev. B **67**, 024429 (2003).
[47] R. Koch, C. Pampuch, H. Yamaguchi, A. K. Das, A. Ney, L. Däweritz, and K. H. Ploog, Phys. Rev. B **70**, 092406 (2004).
[48] R. F. S. Hearmon, *Elastic, Piezoelectric and Related Constants of Crystals*, Landolt-Börnstein, New Series, Group III, Vol. 2 (Springer-Verlag, Berlin, 1969).
[49] J. Donnay and H. Ondik, *Crystal data* (National Bureau of Standards, Gaithersburg, MD, 1973).
[50] J. Zarestky and C. Stassis, Phys. Rev. B **35**, 4500 (1987).
[51] M. Kottcke and K. Heinz, Surf. Sci. **376**, 352 (1997).
[52] K. Dahmen, H. Ibach, and D. Sander, J. Magn. Magn. Mater. **231**, 74 (2001).
[53] K. Dahmen, S. Lehwald, and H. Ibach, Surf. Sci. **446**, 161 (2000).
[54] M. Komelj and M. Fahnle, Phys. Rev. B **65**, 212410 (2002).
[55] D. Sander, A. Enders, C. Schmidthals, D. Reuter, and J. Kirschner, Surf. Sci. **402-404**, 351 (1998).
[56] R. Popescu, H. L. Meyerheim, D. Sander, J. Kirschner, P. Steadman, O. Robach, and S. Ferrer, Phys. Rev. B **68**, 155421 (2003).
[57] L. Hammer, W. Meier, A. Klein, P. Landfried, A. Schmidt, and K. Heinz, Phys. Rev. Lett. **91**, 156101 (2003).
[58] G. Gilarowski, J. Méndez, and H. Niehus, Surf. Sci. **448**, 290 (2000).
[59] Z. Tian, Ph. D. thesis, Martin-Luther-Universität, Halle-Wittenberg, 2008.
[60] D. Sander, A. Enders, and J. Kirschner, Europhys. Lett. **45**, 208 (1999).
[61] V. Martin, W. Meyer, C. Giovanardi, L. Hammer, K. Heinz, Z. Tian, D. Sander, and J. Kirschner, Phys. Rev. B **76**, 205418 (2007).
[62] U. Gradmann and G. Waller, Surf. Sci. **116**, 539 (1982).
[63] D. Sander, A. Enders, and J. Kirschner, J. Magn. Magn. Mater. **200**, 439 (1999).
[64] T. Gutjahr-Löser, D. Sander, and J. Kirschner, J. Magn. Magn. Mater. **220**, 1 (2000).
[65] W. Wulfhekel, T. Gutjahr-Löser, F. Zavaliche, D. Sander, and J. Kirschner, Phys. Rev. B **64**, 144422 (2001).
[66] T. Gutjahr-Löser, D. Sander, and J. Kirschner, J. Appl. Phys. **87**, 5920 (2000).
[67] O. Thomas, Q. Shen, P. Schieffer, N. Tournerie, and B. Lépine, Phys. Rev. Lett. **90**, 017205 (2003).
[68] G. Wedler, B. Wassermann, and R. Koch, Phys. Rev. B **66**, 064415 (2002).
[69] M. Ciria, J. I. Arnaudas, A. del Moral, and R. C. O'Handley, Phys. Rev. B **70**, 054431 (2004).
[70] M. Komelj and M. Fähnle, J. Magn. Magn. Mater. **220**, 8 (2000).
[71] M. Komelj and M. Fähnle, J. Magn. Magn. Mater. **224**, 1 (2001).
[72] M. Fähnle, M. Komelj, R. Q. Wu, and G. Y. Guo, Phys. Rev. B **65**, 144436 (2002).
[73] M. Komelj and M. Fähnle, Phys. Rev. B **65**, 092403 (2002).
[74] G. Y. Guo, D. J. Roberts, and G. A. Gehring, Phys. Rev. B **59**, 14466 (1999).
[75] G. Y. Guo, J. Magn. Magn. Mater. **209**, 33 (2000).
[76] G. Busch, M. Campagna, and H. C. Siegmann, Phys. Rev. B **4**, 746 (1971).
[77] M. B. Stearns, *Magnetic Properties of Metals*, Landolt-Börnstein, New Series, Group III, Vol. 19 Pt. A (Springer, New York, 1984).